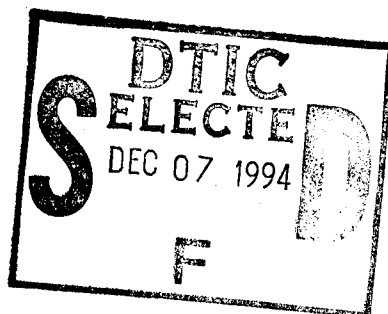WL-TR-94-3012

THE EFFECT OF PRESSURE GRADIENTS ON TRANSITION ZONE LENGTH IN HYPERSONIC BOUNDARY LAYERS

R. L. KIMMEL

DECEMBER 1993

FINAL REPORT FOR 06/01/90 - 12/01/93

APPROVED FOR PUBLIC RELEASE; DISTRIBUTION IS UNLIMITED

FLIGHT DYNAMICS DIRECTORATE
WRIGHT LABORATORY
AIR FORCE MATERIEL COMMAND
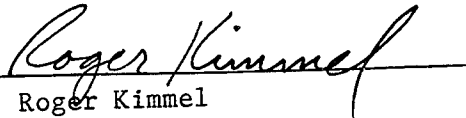WRIGHT PATTERSON AFB OH 45433-7562
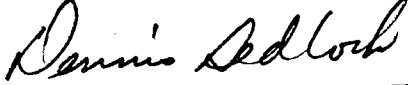
19941201 054

NOTICE

When Government drawings, specifications, or other data are used for any purpose other than in connection with a definitely Government-related procurement, the United States Government incurs no responsibility or any obligation whatsoever. The fact that the government may have formulated or in any way supplied the said drawings, specifications, or other data, is not to be regarded by implication, or otherwise in any manner construed, as licensing the holder, or any other person or corporation; or as conveying any rights or permission to manufacture, use, or sell any patented invention that may in any way be related thereto.

This report is releasable to the National Technical Information Service (NTIS). At NTIS, it will be available to the general public, including foreign nations.

This technical report has been reviewed and is approved for publication.

Roger Kimmel
Aerospace Engineer
Aerothermodynamics and Flight
Mech Research Branch

Valentine Dahlem, Chief
Aerothermodynamics and Flight
Mech Research Branch

Dennis Sedlock, Acting Chief
Aeromechanics Division

If your address has changed, if you wish to be removed from our mailing list, or if the addressee is no longer employed by your organization please notify WL/FIMH , WPAFB, OH 45433- 7936 to help us maintain a current mailing list.

Copies of this report should not be returned unless return is required by security considerations, contractual obligations, or notice on a specific document.

REPORT DOCUMENTATION PAGE

Public reporting burden for this collection of information is estimated to average 1 hour per response, including the time for reviewing instructions, searching existing data sources, gathering and maintaining the data needed, and completing and reviewing the collection of information. Send comments regarding this burden estimate or any other aspect of this collection of information, including suggestions for reducing this burden, to Washington Headquarters Services, Directorate for Information Operations and Reports, 1215 Jefferson Davis Highway, Suite 1204, Arlington, VA 22202-4302, and to the Office of Management and Budget, Paperwork Reduction Project (0704-0188), Washington, DC 20503.

1. AGENCY USE ONLY (Leave blank)	2. REPORT DATE DEC 1993	3. REPORT TYPE AND DATES COVERED FINAL 06/01/90--12/01/93

4. TITLE AND SUBTITLE THE EFFECT OF PRESSURE GRADIENTS ON TRANSITION ZONE LENGTH IN HYPERSONIC BOUNDARY LAYERS

6. AUTHOR(S) R.L. KIMMEL

5. FUNDING NUMBERS
C
PE 61102F
PR 2307
TA N4
WU 63

7. PERFORMING ORGANIZATION NAME(S) AND ADDRESS(ES)

FLIGHT DYNAMICS DIRECTORATE
WRIGHT LABORATORY
AIR FORCE MATERIEL COMMAND
WRIGHT PATTERSON AFB OH 45433-7562

8. PERFORMING ORGANIZATION REPORT NUMBER

9. SPONSORING/MONITORING AGENCY NAME(S) AND ADDRESS(ES)
FLIGHT DYNAMICS DIRECTORATE
WRIGHT LABORATORY
AIR FORCE MATERIEL COMMAND
WRIGHT PATTERSON AFB OH 45433-7562

10. SPONSORING/MONITORING AGENCY REPORT NUMBER
WL-TR-94-3012

11. SUPPLEMENTARY NOTES

12a. DISTRIBUTION/AVAILABILITY STATEMENT
APPROVED FOR PUBLIC RELEASE; DISTRIBUTION IS UNLIMITED.

12b. DISTRIBUTION CODE

13. ABSTRACT (Maximum 200 words)

Boundary layer transition was measured in zero, favorable, and adverse pressure gradients at Mach 8 using heat transfer. Models consisted of 7° half angle forecones 0.4826 m long, followed by flared or ogive aft bodies 0.5334 m long. The flares and ogives produced constant pressure gradients. For the cases examined, favorable pressure gradients delay transition and adverse pressure gradients promote transition, but transition zone lengths are shorter in favorable pressure gradient. Results of the effect of adverse pressure gradient on transition zone lengths were inconclusive.

14. SUBJECT TERMS
HYPERSONICS, TRANSITION, TURBULENCE, BOUNDARY LAYERS, HEAT TRANSFER

15. NUMBER OF PAGES 43

16. PRICE CODE

17. SECURITY CLASSIFICATION OF REPORT	18. SECURITY CLASSIFICATION OF THIS PAGE	19. SECURITY CLASSIFICATION OF ABSTRACT	20. LIMITATION OF ABSTRACT
UNCLASSIFIED	UNCLASSIFIED	UNCLASSIFIED	UL

Contents

List of Figures

List of Tables

PREFACE

NOMENCLATURE

a_i	$=$	coefficients for 5th order polynomial fillet (Table 2.2)
B	$=$	pressure gradient parameter, $(L/C_{pc})(dC_p/dx)$, (Table 2.2)
C_p	$=$	pressure coefficient, $(p - p_\infty)/q_\infty$
DPDX	$=$	Nominal non-dimensional pressure gradient
G	$=$	Görtler number, $Re_\theta\sqrt{\theta/R}$
h	$=$	specific enthalpy of air, kJ/kg
L	$=$	model length, 1.016 m
M	$=$	Mach number
m	$=$	Coefficient in power-law body description (Table 2.2)
p	$=$	pressure, kPa
q	$=$	dynamic pressure, $1/2\rho U^2$
$\dot{q}$	$=$	heat transfer rate per unit area, W/m^2
R	$=$	model radius of curvature, m
Re	$=$	Reynolds number, $Re_{u\delta} \cdot s$
Re_u	$=$	Unit Reynolds number, m^{-1}
Re_θ	$=$	Reynolds number based on momentum thickness, $Re_{u\delta} \cdot \theta$
r	$=$	model cross-sectional radius, m
s	$=$	arc length along model surface, m
St	$=$	Stanton number, $\dot{q}/(\rho_\infty U_\infty(h(T_0) - h(T_w)))$
T	$=$	Temperature, K
U	$=$	velocity, m/s
x	$=$	distance along model longitudinal axis, m
x_c	$=$	reference length, 0.508 m $= L/2$
α	$=$	angle of attack
ρ	$=$	density, kg/m^3
θ	$=$	cone half angle, 7°, also boundary layer momentum thickness, m
ϕ	$=$	model roll angle

Subscripts

b	$=$	beginning of transition

c	$=$	conical forebody
e	$=$	end of transition
tr	$=$	transition
w	$=$	wall
∞	$=$	freestream conditions upstream of model bow shock
0	$=$	stagnation conditions
δ	$=$	boundary layer edge
ΔRe	$=$	$Re_e - Re_b$
θ	$=$	boundary layer momentum thickness

Section 1

INTRODUCTION

Boundary layer transition has a strong impact on hypersonic vehicles through the increase in heat transfer and skin friction associated with it. The transitional region between the end of fully laminar flow and the beginning of fully turbulent flow can be of the same length as the laminar zone preceding it. These factors combine to place a premium on accurate prediction of the transitional flow region. In particular, the effect of pressure gradient is of concern, since most realistic flight vehicles contain regions of pressure gradient.

A great deal of experimental work exists on the transition zone in low speed flow [1]. Much of the work regarding pressure gradient effects is oriented toward turbomachinery. Numerous studies of hypersonic boundary layer transition have been conducted over the years. Most of these studies have dealt with the beginning or end of transition, not with the transitional zone itself. Jack [2] examined the effect of favorable pressure gradient on transition on bodies of revolution at Mach 3.12. Published recovery temperature data from this test do not show a clear trend. Jack tested configurations which produced constant favorable pressure gradients $d(p/p_\infty)/dx$ of 0, -0.002, and -0.004 per mm, which produced normalized transition lengths, x_e/x_b, of 2.6, 1.7, and 3.6, respectively. Zakkay, et al. [3] investigated a cone-flare configuration at Mach 10. Since only one flare configuration was tested, it is not possible to extract trends from their experiment.

Lower Mach number studies are of interest because the physics of the transition process have been explored more fully, and because of the high quality flight and quiet wind tunnel data available. Transition at low speeds is ascribed to the formation of turbulent spots which originate in a fairly narrow band of Reynolds numbers, and which grow and convect downstream until they coalesce into a fully turbulent boundary layer, as described by Em-

1

mons [4]. The region between the beginning of the spots and their complete coalescence into turbulence is marked by a streamwise-varying intermittency between laminar and turbulent flow. This intermittency averages over time to give a smooth spatial transition from laminar to turbulent flow properties. The effect of a parameter such as pressure gradient is manifested in the length of the mean transitional zone by its effect on spot characteristics such as generation rate and spreading angle. The available evidence on subsonic flat plate transition indicates that adverse pressure gradient shortens the transition zone length, and favorable pressure gradient lengthens it [5, 6, 7]. Dhawan and Narasimha [8] and Potter and Whitfield [9] have compiled data showing a trend of increasing transition zone Reynolds number, $\Delta Re = (Re_e - Re_b)$, with increasing transition Reynolds number, Re_b, for freestream Mach numbers less than 8. Both compilations, however, show that Re_e increases at a slower rate than Re_b, so that the ratio Re_e/Re_b decreases slightly as Re_b increases. Potter and Whitfield show x_e/x_b ranging from 1.2 to 1.6, with x_e/x_b increasing as Mach number increases.

One of the most detailed boundary layer transition studies was the AEDC transition cone, a sharp, 5° half angle cone, which was tested in a variety of facilities and in free-flight [10, 11]. The cone was tested at freestream Mach numbers up to 5.2 in ground testing, but up to only approximately Mach 2 in flight. The cone was adiabatic, and the detection method was surface Pitot pressure probe. Normalized transition zone lengths in free-flight were $1.1 \leq x_e/x_b \leq 1.2$. Some ground tests match the flight test results, but results vary from facility-to-facility, and typically give longer transition zone lengths than freeflight, up to 2.3. At the highest Mach number reported in reference [11], 4.4, x_e/x_b was 1.5.

In general, subsonic and supersonic data show that the transition zone length increases as ambient noise increases, either in ground test or freeflight. Data from the NASA Langley Mach 3.5 pilot quiet tunnel at $M_\infty = 3.5$ on a 5° half angle sharp cone also showed transition zone lengths of 1.1 to 1.2 under quiet conditions [12]. Noise in this facility produced normalized zone lengths of 1.3 to 1.6. Sharp leading edge flat plates also showed transition zone lengths of 1.1 to 1.2 under quiet conditions, but interestingly, the transition zone length was unaffected by noise. Data on blunt cones in this facility showed a weak trend of increasing transition zone length with increasing nose bluntness up to the maximum bluntness Reynolds number of 10^5. Insufficient data were obtained on blunt plates to observe a bluntness trend.

The lower Mach number data provide some clues as to what the hypersonic transition zone may look like, but cannot arbitrarily be applied to hypersonic boundary layers. Transition zone phenomena, even in zero pres-

sure gradient flow, are less clearly defined at hypersonic speeds. James [13], Fischer [14], and Havener [15] have observed turbulent spot formation optically at hypersonic Mach numbers up to 9, but no quantitative measurements of hypersonic turbulent bursts exist. Owen, et al. [16] have measured intermittency using thin film gauges at a freestream Mach number of 7.

Although the assumption of $x_e/x_b = 1.1$ to 1.2 based on subsonic and supersonic data is conservative from a design point of view, one cannot necessarily expect the transition zone length to remain constant as Mach number increases. As Mach number increases, the boundary layer becomes more stable, in the sense that first and second mode amplification rates decrease with increasing Mach number [17]. Also, the spreading rate of turbulent free shear layers has been shown to decrease with increasing Mach number [18]. Potter and Whitfield [9] show a trend of increasing transition zone length with increasing Mach number, up to Mach 8. The hypersonic transition zone length in zero pressure gradient is often assumed to be approximately two. Data in references [16, 19, 20, 21, 22, 23, 24, 25, 26, 27] on cones and flat plates show a range of transition zone lengths, x_e/x_b, from 1.6 to 2.5. These experimenters used a variety of transition detection techniques including surface hot film, heat transfer, and recovery temperature measurements. In addition, the different transition detection techniques used make it difficult to compare results from different tests. The wall-to-stagnation temperature ratio was varied in two of these experiments [20, 22] and had little effect on the transition zone length. All of these experiments were done in conventional hypersonic facilities. Hypersonic free-flight data compiled by Wright and Zoby [28] for comparison with the Reentry-F flight experiment showed transition zone lengths from 1.5 to 1.9. Reentry-F itself showed varied behavior as altitude and nose bluntness changed over time. Transition zone length on Reentry F varied from 1.6 to 2.0 over most of the trajectory, but increased greatly at lower altitudes, reaching a maximum of 5.4. Hypersonic flight data are difficult to interpret because, in addition to the usual flight test problems of vehicle attitude, etc., hypersonic vehicles tend to have blunt, ablating noses [29]. Experiments by Stetson [27] on an 8° half angle cone at $M_\infty = 6$ showed that the transition zone length x_e/x_b decreased approximately 6% as nose bluntness increased from 0 to 0.2 inch radius (Reynolds number based on freestream properties and nose radius of 3.2×10^5).

The goal of the experiment reported in this paper was to perform detailed hot wire measurements in the boundary layer to examine the effect of pressure gradient on second mode instabilities. The transition data obtained during the test were a by-product of these measurements, and as such the test was not optimized for transition measurement. However, given the paucity of

3

data on hypersonic transition lengths, the transition data are being presented in their own right.

Section 2

EXPERIMENT

Tests were conducted at Arnold Engineering Development Center (AEDC) Tunnel B at a nominal freestream Mach number of 7.93. Models with nominal non-dimensional pressure gradients (DPDX) of -2, -1, 0, 1, and 4 were tested at a variety of unit Reynolds numbers. The test matrix is summarized in Table 2.1. The baseline, zero pressure gradient model was tested in 1979 and 1985, the adverse pressure gradient models were tested in 1990, and the favorable pressure gradient models were tested in 1992. Details of the zero pressure gradient tests, which consist primarily of hot wire data, are presented in Reference [30].

The baseline model (configuration 0) consisted of a 7° half angle, sharp-nosed cone. The pressure gradient models consisted of a single conical forebody, 0.4826 m long, and interchangeable flared or ogive after-bodies 0.5334 m long (configurations -2, -1, 1, and 4). In the adverse pressure gradient models, the flare turning angle was constrained so that at the base of the model with maximum turning (configuration 4), the model contour would be no more than approximately half way between the configuration 0 contour and the configuration 0 shock. This ensured that the model bow shock would not intersect the aft-body. The favorable pressure gradient model turning was constrained so that at the base of the model with maximum turning, the model contour was approximately tangent to a cylinder.

The flare and ogive contours were calculated to provide constant pressure gradients. The configuration nomenclature is derived from the nominal non-dimensional pressure gradient parameter, $(L/C_{pc})(dC_p/dx)$. Configuration 1, for example, is so named because its gradient would produce a 100% rise above the cone pressure coefficient, C_p, over the model reference length L, 1.016 m. Since the flare length was 50% of the model length, the pressure coefficient rose 50% above the cone level by the end of the model. Configura-

5

tion 4 had a nominal 200% increase in pressure coefficient by the end of the model. Configurations -1 and -2 achieved nominal 50% and 100% pressure coefficient drops, respectively, by the ends of the models. All models were constructed of stainless steel, with approximately 6.4 mm wall thickness. The nose radius was nominally 0.05 mm.

The design of the models is described in References [31] and [32]. The power-law configuration, where body radius is proportional to the mth power of x, was chosen to describe the aft-body contours. The power-law was chosen because in Newtonian impact theory, the power law with $m = 1.5$ produces a constant pressure gradient [33]. The basic power law exponent was varied to give a constant gradient based on Parabolized Navier Stokes (PNS) computations. PNS computations described in [31] and [32] showed that $m = 1.5$ was sufficient for configurations 1 and - 1, but for configuration 4, the exponent m was reduced to 1.43. The pressure gradient for configuration - 2 was reduced in magnitude to -1.9, and the exponent m was increased to 1.595, reflecting the increased displacement thickness growth on this configuration.

A quintic fillet between the end of the cone at $x/L = 0.475$ and the beginning of the power law aft-body at $x/L = 0.550$ was chosen to match radius, first, and second derivatives between the cone and the flare. Although the second derivative at the fillet-flare juncture was matched, the slope of the second derivative at this point was discontinuous. This produces an overshoot in the pressure gradient, but computations [31] showed the overshoot to be less than 10% of the desired gradient. The complete equations for the flare geometries are given in Table 2.2, where the magnitude of the pressure gradient is given by the coefficient B. The model geometries and radii of curvature are given in Figures 2.1 and 2.2.

The models were instrumented with pressure taps and Schmidt-Boelter heat transfer gauges. Model surface temperature was measured directly from the Schmidt-Boelter gauges. Pressure taps and heat transfer gauges were installed at 50.8 mm intervals from $x/L = 0.300$ to $x/L = 0.450$, inclusive, on the cone, and at 25.4 mm intervals between $x/L = 0.550$ and $x/L = 0.925$, inclusive, on the power-law aft- body. Pressure taps and heat transfer gauges were installed on the 180° and 90° meridians, respectively. Heat transfer measurements were made by injecting the model, measuring heat transfer, and removing the model immediately before significant heating occurred. Several measurements were made at each unit Reynolds number in the test matrix. Between measurements, the model was cooled to nominal room temperature. The nominal wall-to-stagnation temperature ratio for all transition measurements was thus 0.42. The hot wire and mean boundary layer surveys were conducted after a heat soak which raised the model to nominal recovery

temperature.

Caveats regarding the data are necessary. Transition Reynolds numbers obtained in the experiment are expected to be lower than free-flight transition Reynolds numbers [26]. However, hot wire measurements obtained in this facility on other conical configurations show that the dominant instability is second mode [30]. Experimental wall cooling, nose bluntness, and Mach number transition trends have been shown to be described qualitatively by linear theory [34]. Thus, at least the instability processes leading up to the beginning of transition are not noise dominated.

Another warning regarding the experiment is that it was designed to obtain stability data, and as such, was not optimized for transition experiments. In particular, the instrumentation is sparse, especially at the cone-power-law juncture. This leads to uncertainty in the transition location, as discussed below. The cone-power-law configuration was chosen so that the pressure gradient would be imposed on second mode waves which had been well-developed on the cone. Because of this, the transition begins at various points either on the cone or the flare, depending on the unit Reynolds number, and thus the transitional region shows varying degrees of influence from the pressure gradient.

The primary sources of inaccuracy in the transition measurements are the accuracy of the heat transfer gauges and the uncertainty in the location of maxima and minima in heat transfer due to spacing of the gauges. Assignment of an accuracy to the gauges is difficult. Reference [35] ascribes an accuracy of $\pm$ 5% to the gauges. Measurements show good run-to-run precision, with variations of less than 1%. An assessment of the gauge accuracy may be obtained by comparing zero pressure gradient laminar heat transfer predictions on the cone to measured heat transfer. Heat transfer predictions for this simple case are reliable enough, especially in predicting trends with x, to serve as an in-situ calibration of the gauges. The measured heat transfer shows some scatter about the predicted values, but most of the gauges fall within the $\pm$ 5% of theoretical band, although some gauges fall outside of this band. A more conservative estimate of transducer accuracy would be $\pm$ 10%.

Uncertainty in the transition beginning and end locations is also difficult to assess. The heat transfer gauge spacing of 50.8 mm on the model forecones places a limit on how well the beginning of transition may be resolved. In practice, the primary source of uncertainty is scatter in the heat transfer values, which makes determination of the maximum and minimum heat transfer locations somewhat subjective. This source of error is also the most difficult to quantify.

Transition beginning will be defined as the minimum in heat transfer, and transition end will be defined as the maximum overshoot in heat transfer above the turbulent values. In the adverse pressure gradient cases, this may only be a local minimum or maximum. Any number of criteria may be used to define the beginning and end of transition, and not all give the same transition Reynolds number or transition zone length [36]. The choice of criteria is largely a matter of convenience. The important point is to use the same criteria when comparing measurements. The use of the minimum in heat transfer is rational in that it is well-defined, of interest from a design viewpoint, and has been shown to coincide with the first departures of boundary layer profiles and fluctuations away from their laminar values [34]. The maximum in heat transfer is also a rational choice for end-of-transition demarcation in that it is well-defined and of design interest. It should be noted that the peak heat transfer probably does not correspond to an equilibrium turbulent boundary layer. Heat transfer does not relax to its equilibrium turbulent values for many boundary layer thicknesses downstream of the peak. Compressible turbulent boundary layers typically take many boundary layer thicknesses to equilibrate after perturbations. Experiments on a turbulent boundary layer at $M_\delta = 3.0$ [37] have shown that velocity profiles in a turbulent boundary layer had not relaxed to equilibrium turbulent profiles even 12δ downstream of a successive compression- expansion perturbation.

Table 2.1: Test Matrix

CONFIGURATION

Re_∞ m^{-1}	-2	-1	0	+1	+4
1.6×10^6 m^{-1}	XX	*	XX	B	B
3.3×10^6 m^{-1}	*	B	B_c	B	B
3.9×10^6 m^{-1}	XX	XX	B_c	XX	XX
4.9×10^6 m^{-1}	B_c, E	B_c, E	XX	B_c, E	B, E
6.6×10^6 m^{-1}	B_c, E	B_c, E	B_c, E	B_c, E	B_c, E
8.2×10^6 m^{-1}	XX	XX	B_c, E	XX	XX

$M_\infty = 7.93$
$T_0 = 722$ K
$T_w/T_0 = 0.42$

XX - Not Tested
*   - Completely laminar
B - Beginning of Transition on model
B_c - Transition beginning on cone
E - End of transition on model

Table 2.2: Model Geometry Coefficients.

CONFIGURATION

Coefficient	-2	-1	+1	+4
B	-1.9	-1.0	1.0	4.0
m	1.595	1.5	1.5	1.43
a_0	-1.760775	-7.747701×10^{-1}	7.584605×10^{-1}	2.502281
a_1	1.779659×10^1	7.901532	-7.498973	-2.505959×10^1
a_2	-7.074643×10^1	-3.114571×10^1	3.054475×10^1	1.010698×10^2
a_3	1.411183×10^2	6.214336×10^1	-6.100083×10^1	-2.021491×10^2
a_4	-1.402110×10^2	-6.176131×10^1	6.068375×10^1	2.014049×10^2
a_5	5.548435×10^1	2.444745×10^1	-2.404474×10^1	-7.992703×10^1

$$\frac{r(x/L)}{L} = \frac{x}{L}\tan(\theta) \qquad \frac{x}{L} \leq 0.475$$

$$\frac{r(x/L)}{L} = a_0 + a_1\left(\frac{x}{L}\right) + a_2\left(\frac{x}{L}\right)^2 + a_3\left(\frac{x}{L}\right)^3 + a_4\left(\frac{x}{L}\right)^4 + a_5\left(\frac{x}{L}\right)^5 \qquad 0.475 \leq \frac{x}{L} \leq 0.55$$

$$\frac{r(x/L)}{L} = \frac{x_c}{L}\tan(\theta) + \frac{\tan(\theta)}{Bm}\{[B(\frac{x}{L} - \frac{x_c}{L}) + 1]^m - 1\} \qquad \frac{x}{L} \geq 0.55$$
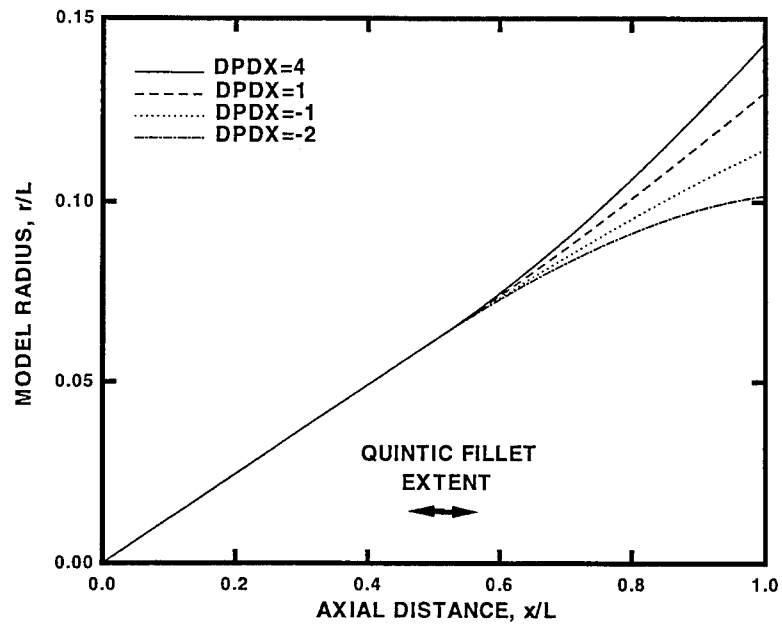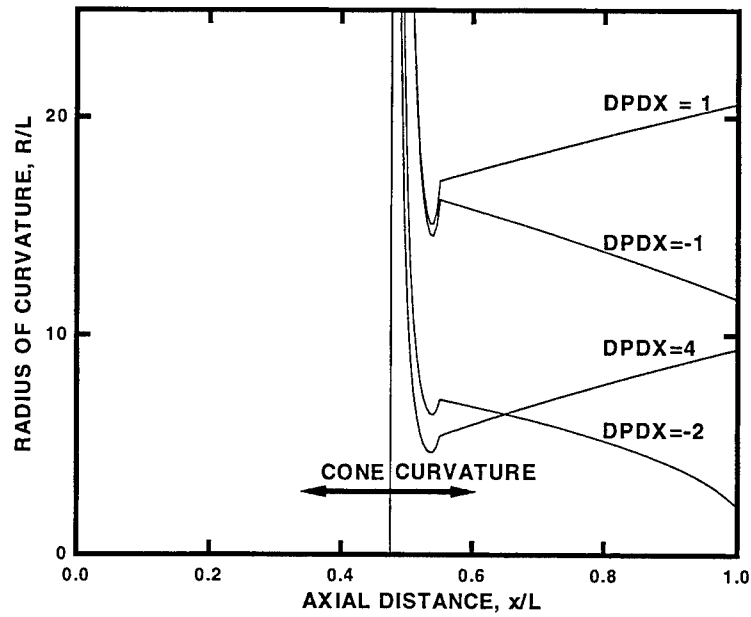
Figure 2.1: Model Geometries.

Figure 2.2: Model Longitudinal Radii of Curvature.

11

Section 3

RESULTS

Surface static pressure results in Figure 3.1 show that the aft-bodies did indeed produce nearly constant pressure gradients. The slope of the pressure rises shown in the figure are measured values obtained by linear regression of the data. Pressure data for roll orientations of 0° and 180° for configuration 1 (Figure 3.2) show that this model was inadvertently installed at angle of attack. Comparison of forecone pressures with the AEDC angle of attack correlations shown in Figure 3.3 for a 7° cone [35] show that the angle of attack of configuration 1 was approximately 0.4° to 0.8°. All heat transfer measurements were made on the leeward side of the model. Calculations of heat transfer and momentum thickness described below assumed zero angle of attack. Data from previous investigators indicate that the beginning and end of transition move forward on the leeward side of a sharp cone at angle of attack [23, 27, 38]. Measurements by Stetson [27] at $\alpha = 0.5°$ on an 8° sharp cone indicate that the transition zone length is not affected by angle of attack.

Surface temperature distributions are shown in Figure 3.4. The models were cooled between runs to provide constant, uniform starting temperature distributions. Some temperature non-uniformities are unavoidable during a heat transfer run due to non-uniform heating rates from boundary layer transition and internal model conduction. The maximum peak-to-peak variation in temperature, however, is less than 5%. Heat transfer results are repeatable and are not significantly affected by the slightly non-uniform surface temperatures.

Edge conditions obtained from boundary layer surveys on the adverse pressure gradient models at a unit Reynolds number of 3.3×10^6 m^{-1} are shown in Figures 3.5 and 3.6. The boundary layer surveys were obtained after the models had heated to adiabatic conditions, but adiabatic wall edge

12

conditions are essentially identical to cooled wall edge conditions. Although velocity is decreasing and viscosity is increasing through the adverse pressure gradient, static density is increasing at a faster rate, so the local unit Reynolds number increases through the pressure gradient. The effect is pronounced on configuration 4, but the increase on configuration 1 is relatively small.

Since only limited flow field surveys were available for the favorable pressure gradient models, their edge conditions were calculated using the measured surface static pressure and the perfect gas relations contained in the BLIMP program (Boundary Layer Integral Matrix Procedure), which is a numerical integral procedure. The BLIMP program is described in Reference [39], and the theory is described in Reference [40]. Comparison of the BLIMP calculations for the adverse pressure gradient configurations lends confidence to the favorable pressure gradient computations. The discrepancy between the configuration 1 measured and calculated values are due to the model angle of attack.

Figure 3.7 shows a typical shadowgraph of the aft section of configuration 4 taken during heat transfer measurements at a freestream unit Reynolds number of 1.6×10^6 m^{-1}. The shadowgraph shows transition at approximately half of the flare length. This "optical" transition occurs over a short spatial extent, approximately half way between the beginning and end of transition as measured from heat transfer. This result is consistent with Demetriades' observation [36]. "Rope" waves were always evident prior to transition, and appear on the zero pressure gradient forecone at higher unit Reynolds numbers. The rope waves showed a packet-like structure, with regions of well-developed waves separated by relatively quiescent flow. No unequivocal evidence of turbulent "bursts" were observed on any of the shadowgraphs. Two to four shadowgraphs were taken at each unit Reynolds number, and they show some frame-to-frame excursion of the transition point, but none show transition or turbulent bursts at the extreme beginning or end of transition as defined by heat transfer. In general, the "optical" transition occurs at different x locations on the upper and lower meridians of the cone, but the variation is random, and there is no consistent asymmetry.

The hot wire spectrum for configuration 4 in Figure 3.8 at $x/L = 0.4$, immediately preceding the flare, shows the presence of a strong second mode component at 150 kHz. This component was identified as second mode by comparison with linear stability results, and it persisted and continued to amplify in the flare region. Previous studies of zero-pressure gradient cooled and uncooled cones in this facility [30, 41] have shown that transition is second-mode dominated.

13

Laminar boundary layer momentum thicknesses for a freestream unit Reynolds number of 1.6×10^6 m^{-1} were calculated using the BLIMP program and used along with the model radius of curvature in Figure 2.2 to calculate Görtler number. This unit Reynolds number was the only one which produced transition on the flare. Figure 3.9 shows that the Görtler numbers at transition were less than 2.3. Incompressible correlations indicate transition for Görtler numbers greater than approximately seven [42]. Studies for quiet wind tunnel nozzle design [43] point out the problems of using such simple correlations for transition prediction, but indicate that a Görtler number of 8-9 is not unreasonable for supersonic quiet nozzle transition. Although various workers have calculated minimum critical Görtler numbers from 0.3 to 1.0 [44, 45], Hall's theoretical results [46] showed that the neutral stability curve depended on how and where the boundary layer was perturbed, so no critical Görtler number was definable. In summary, given the calculated Görtler number and the significant measured second mode component, the transition in this case was probably not Görtler dominated, but Görtler instability may have been present.

The heat transfer data in their entirety are plotted in Figures 3.10 to 3.14. The Reynolds numbers in the figures are based on local boundary layer edge unit Reynolds number and arc length along the model. Laminar and turbulent heat transfer for all configurations was calculated using BLIMP. Laminar heating at the lowest unit Reynolds number tested for each configuration and turbulent heating at the highest unit Reynolds number tested for each configuration, as calculated with the BLIMP program, are shown for comparison. For all calculations, the origin of the turbulent boundary layer was taken at the cone apex. This will result in some error in the magnitude of predicted heat transfer in the turbulent region. However, the goal of the computations was only to provide accurate trends of heat transfer versus x to aid in transition location determination, not to provide accurate heat transfer magnitudes. Laminar heat transfer in zero pressure gradient is proportional to the $-1/2$ power of x, as expected. Turbulent data show more scatter, but have roughly a $-1/5$ power dependence for zero pressure gradient.

Heat transfer trends in the presence of pressure gradient are more complex. An adverse pressure gradient in incompressible flow causes boundary layer thickness to increase and heat transfer to decrease compared to zero-pressure gradient values, but the opposite trends occur in compressible flow. This is primarily because of streamtube compression and expansion and Mach number changes due to pressure gradients in compressible flow. Consequently, wall shear and heat transfer will decrease more slowly with x in an adverse pressure gradient than in zero pressure gradient, however,

14

a strong enough adverse gradient will cause heat transfer and wall shear to increase in the x-direction. The opposite trends occur in a favorable pressure gradient. For laminar flow on configuration 1, heat transfer still decreases in the x-direction, but at a slower rate than the zero pressure gradient case. For turbulent flow on configuration 1 and laminar flow on configuration 4, the heat transfer rises slightly with x. For turbulent flow on configuration 4, heat transfer rises with increasing x. On the favorable pressure gradient cases, heat transfer drops below the zero pressure gradient values.

Because of the scatter in the heat transfer data, it is difficult to determine where the heat transfer is at a true minimum or maximum. Minima and maxima were thus determined using fifth-order, least squares polynomial curvefits of the data. The fifth-order polynomial was chosen as the simplest function which would give a realistic fit of the data. Although the precise beginning and end of transition are still open to some interpretation, the curve fitting technique provided a more consistent interpretation of the data. Note that both the transition measurement technique and the definition of beginning and end affect the transition zone length.

Beginning of transition occurs on configurations 0, 1, and 4 at the lowest unit Reynolds numbers tested for these cases, 3.3×10^6 m^{-1} for configuration 0 and 1.6×10^6 m^{-1} for configurations 1 and 4. Configurations -1 and -2 were entirely laminar at the lowest unit Reynolds numbers at which they were tested, 1.6 and 3.3×10^6 m^{-1}, respectively. End of transition is achieved on configuration 0 at unit Reynolds numbers of 6.6×10^6 m^{-1} and above. End of transition is achieved on the pressure gradient configurations at unit Reynolds numbers of 4.9 and 6.6×10^6 m^{-1}. At these Reynolds numbers, transition begins on the model forecone, so the initial instability growth and at least part of the transition process occurs in zero pressure gradient. Heat transfer overshoots the predicted turbulent values and relaxes to the turbulent trend downstream in all of the pressure gradients.

Heat transfer data for freestream unit Reynolds numbers of 6.6 and 4.9×10^6 m^{-1} are plotted in Figures 3.15 and 3.16 with pressure gradient as a parameter. The line fairings through the data in these figures are the polynomial fits. The data for configuration 1 do not follow the trends of the other configurations, and the beginning and end of transition are biased upstream compared to the other cases. These effects are probably due to the model angle of attack. Data indicate that both the beginning and end of transition move forward on the leeward side of a sharp cone at angle of attack [27, 38], and the amount of forward movement on configuration 1 in Figures 3.15 and 3.16 is consistent with the model being at 0.4° to 0.8° angle of attack, based on data in Reference [38].

15

Since transition begins at approximately the same location on the forecone for all the other pressure gradient models at these Reynolds numbers, the end-of-transition marker provides a direct measure of transition zone length. In all cases, increasing favorable pressure gradient causes decreasing transition length. Results for the adverse pressure gradients do not show such a clear trend. For a unit Reynolds number of 6.6×10^6 m^{-1}, configuration 4 has a longer transition length than the zero pressure gradient case. No heat transfer data were available for the zero pressure gradient case at a unit Reynolds number of 4.9×10^6 m^{-1}, but interpolation of the data indicate that end-of-transition would be at approximately $x/L = 1$. The adverse pressure gradient causes a decrease in transition length at this unit Reynolds number.

Transition beginning and end are plotted in terms of arc length along the model in Figure 3.17 and Reynolds number in Figure 3.18. When the unit Reynolds numbers were low enough for transition to begin on the curved surface of the model, the favorable gradients delayed transition, and the adverse gradients promoted it, as expected.

Transition zone length is plotted in terms of length and Reynolds number in Figures 3.19 and 3.20. The DPDX=0 transition end is consistently 2.2 times the laminar length. The favorable pressure gradient transition zone length is shorter, from approximately 1.7 for configuration -2 to 2.0 for configuration -1. When the data are plotted in terms of Reynolds number, this trend is exaggerated due to the drop in unit Reynolds number with x. Data for the adverse gradients are inconclusive in terms of transition length, but transition end Reynolds numbers generally seem higher than in zero pressure gradient, due to the increase in local unit Reynolds number. The comparison in terms of Reynolds number is somewhat misleading, due to history effects. Although the Reynolds number at the end of configuration 4 at a freestream unit Reynolds number of 6.6×10^6 m^{-1} is 12×10^6, the boundary layer is not representative of a boundary layer which has evolved to this Reynolds number at constant edge conditions, but instead probably retains characteristics of a boundary layer at lower Reynolds number.

The observed trends of shorter transition length with favorable pressure gradient are opposite to what would be expected based on subsonic results, and two factors may contribute. The first factor is that turbulent heat transfer for favorable pressure gradients is lower than zero pressure gradient heat transfer, and adverse pressure gradient heat transfer is higher. For cases where transition began on the forecone, pressure gradient seemed to have little effect on the rate of increase in transitional heat transfer with x. This means that heat transfer would reach turbulent values more quickly in favor-

16

able pressure gradient, and more slowly in adverse pressure gradient (Figure 3.21). In cases where transition begins on or near the flare, however, pressure gradient does have some influence on the rate of increase in transitional heat transfer, with adverse pressure gradient causing a faster rate of increase, and vice versa. In these cases, the net result depends on whether the rate of increase in heat transfer is great enough to overcome the effect of higher turbulent values. With these competing effects, there is no compelling reason to expect simple trends in transition zone length with pressure gradient.

A second factor which may explain trends in transition length is body curvature effects, if one postulates that transition in these hypersonic cases is due to turbulent spot spreading. Limited evidence in supersonic transition on cones [47] and subsonic transition [48] on swept wings indicates that turbulent spots spread at a constant angle with respect to the streamline passing through their origin, not with respect to local streamlines. This would encourage shorter transition lengths on the favorable pressure gradient models, since their surface area is growing at a slower rate in the x-direction compared to the cone, which means that their surface would be covered by a spot more quickly. The converse is true of the adverse pressure gradients. This argument will remain purely speculative until more detailed measurements of the transition process are made, but it does indicate that the results of this paper may not be directly relevant to planar geometries. Quiet wind tunnel results at Mach 3.5, however, show little difference between cone and flat plate transition extent [12].
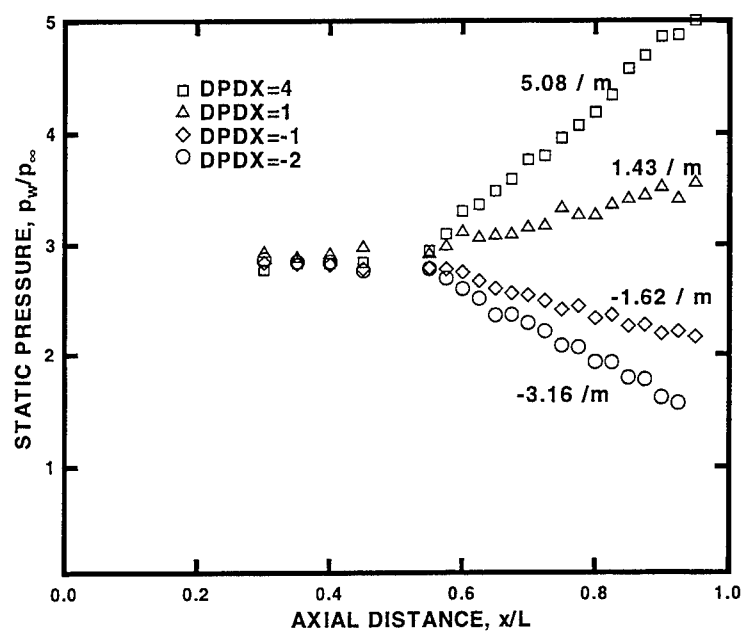
Figure 3.1: Static Pressure Distribution.
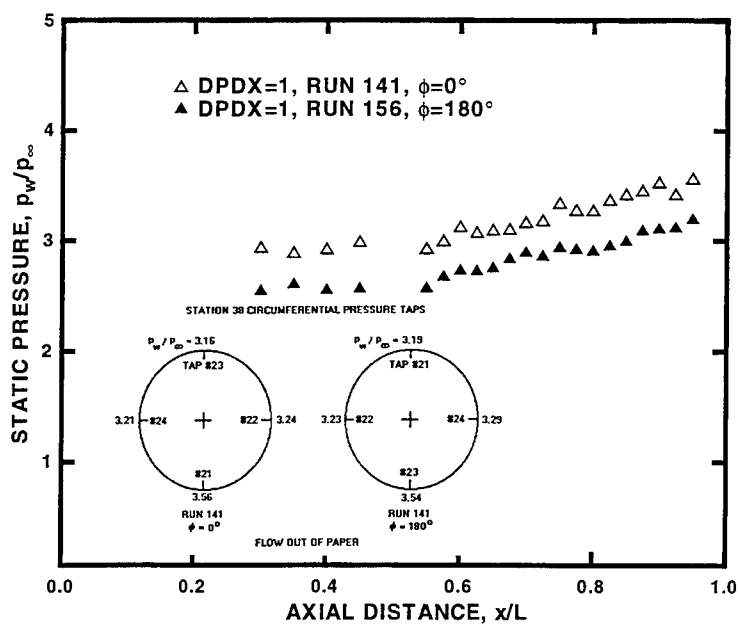
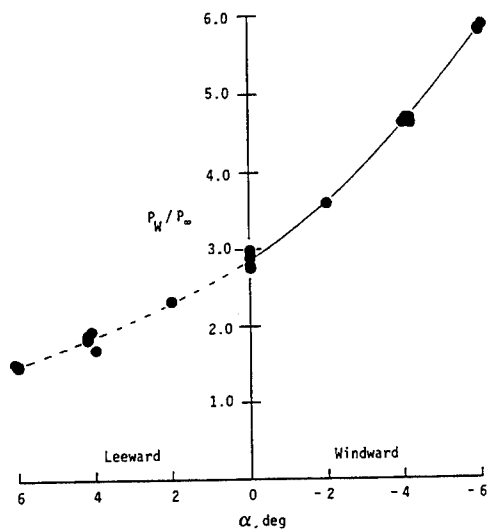Figure 3.2: Configuration 1 Static Pressures, $\phi = 0°$ and $180°$.

18

Figure 3.3: Static Pressure Variation with Angle of Attack, 7° Cone.
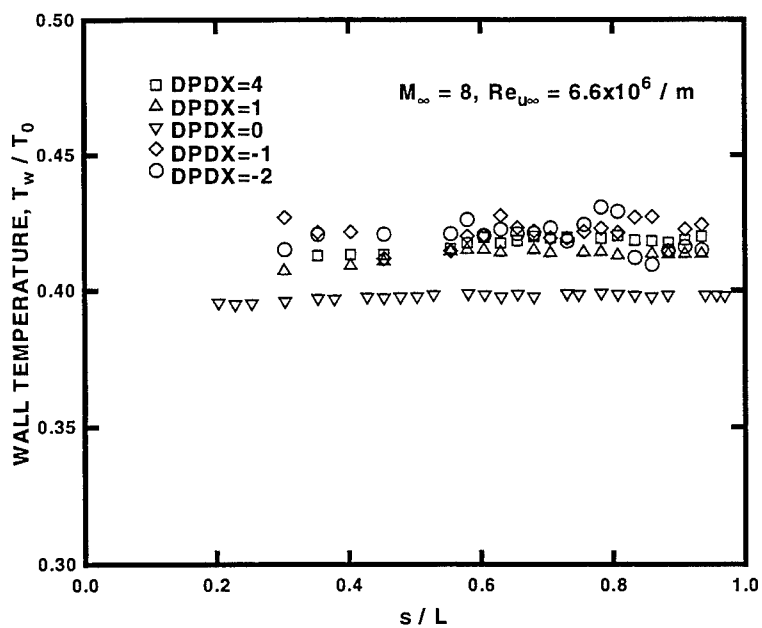

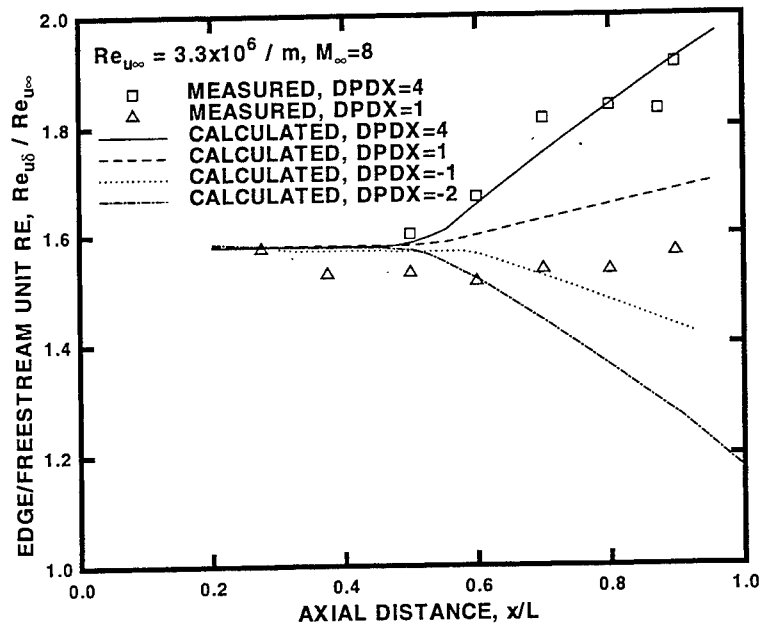Figure 3.4: Wall Temperature Distribution.

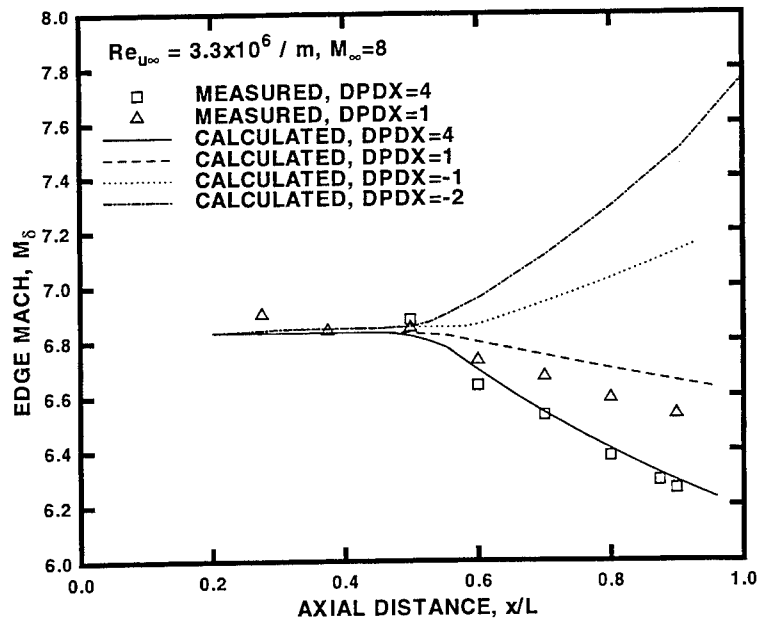Figure 3.5: Boundary Layer Edge Unit Reynolds Numbers.
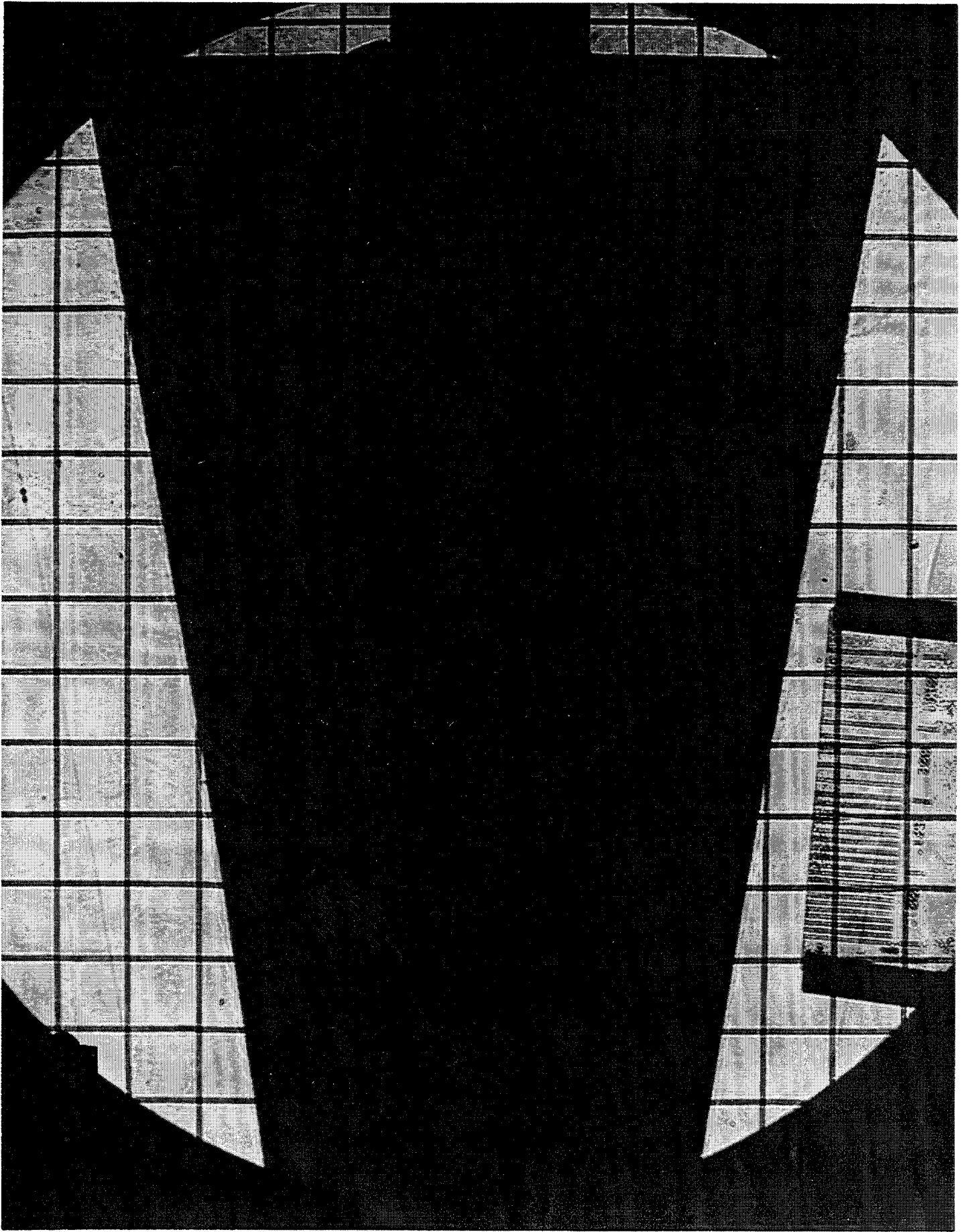

Figure 3.6: Boundary Layer Edge Mach Numbers.

20

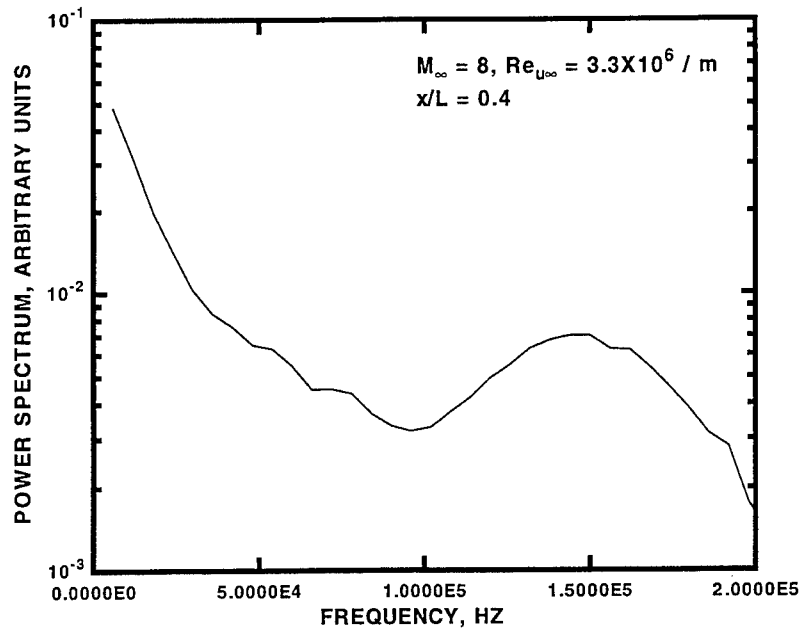Figure 3.7: Shadowgraph of DPDX=4 Configuration, $Re_{u\infty} = 3.3 \times 10^6 \text{ m}^{-1}$

Figure 3.8: Configuration 4 Hot Wire Spectrum, $x/L = 0.4$.
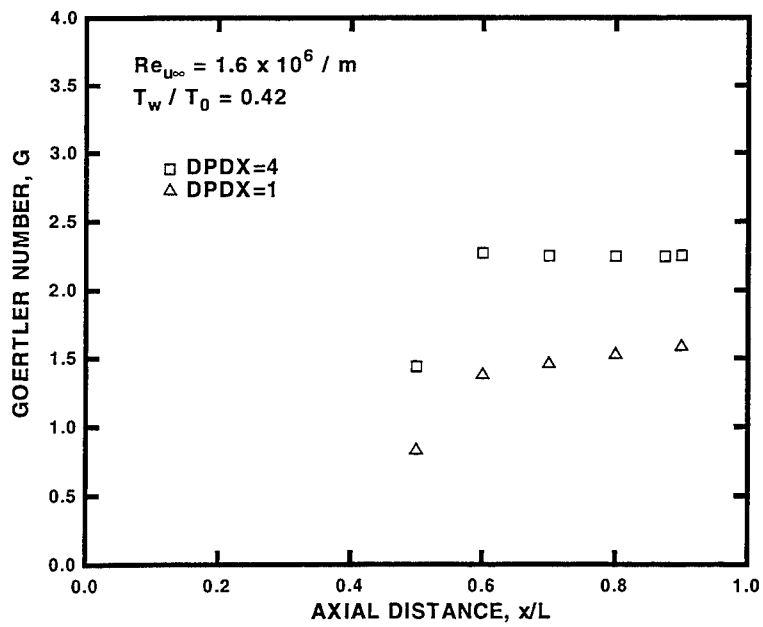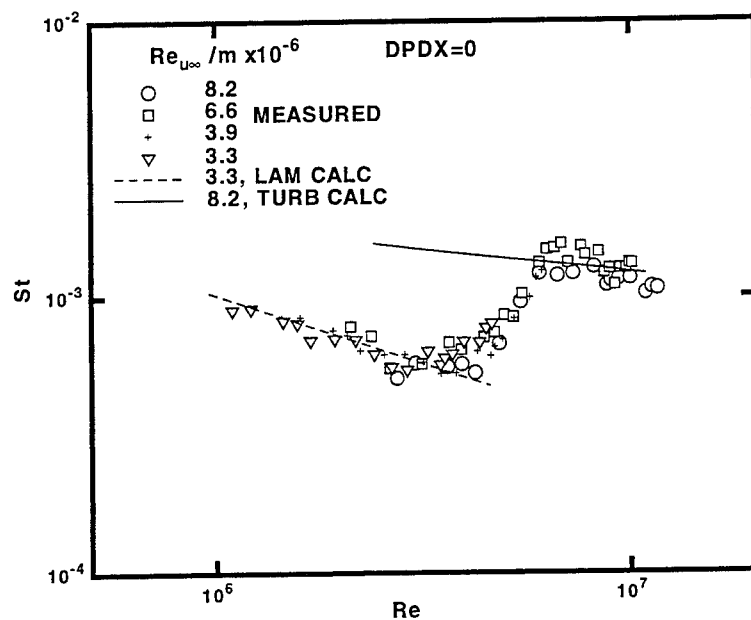

Figure 3.9: Görtler Number

22
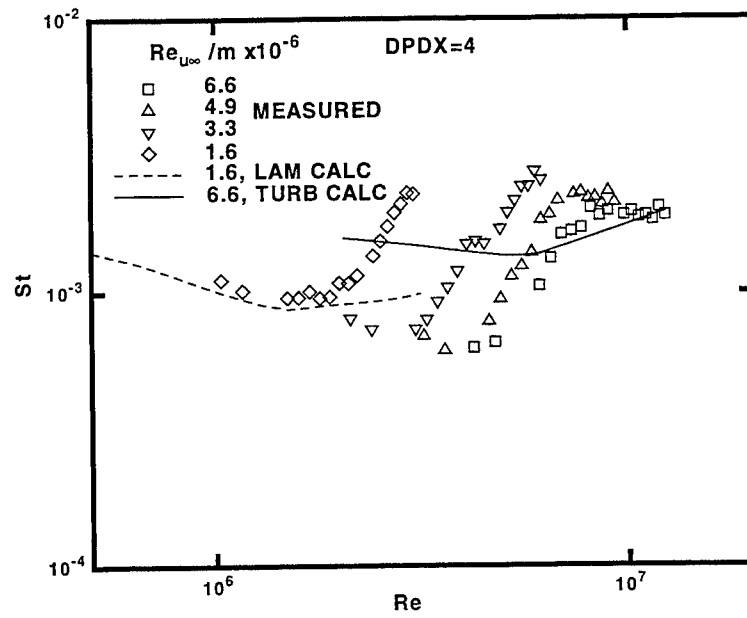
Figure 3.10: Heat Transfer, DPDX=4 Configuration.
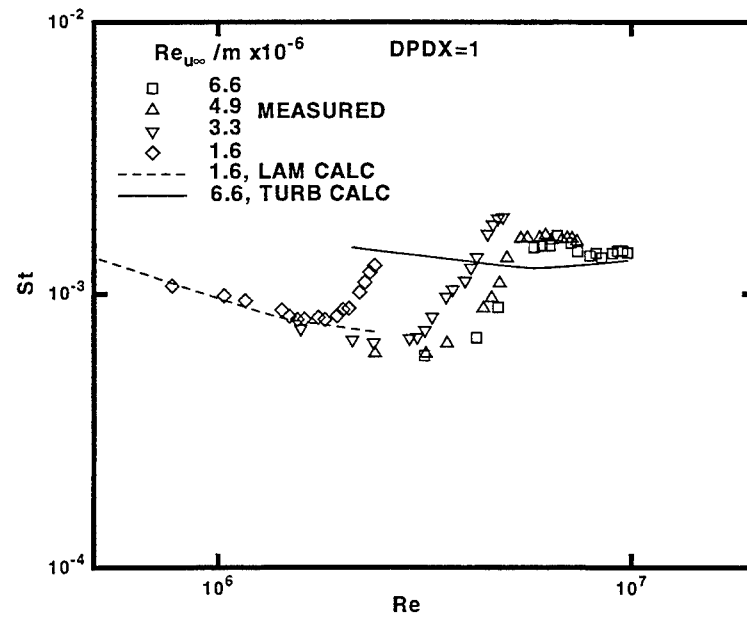
Figure 3.11: Heat Transfer, DPDX=1 Configuration.

23

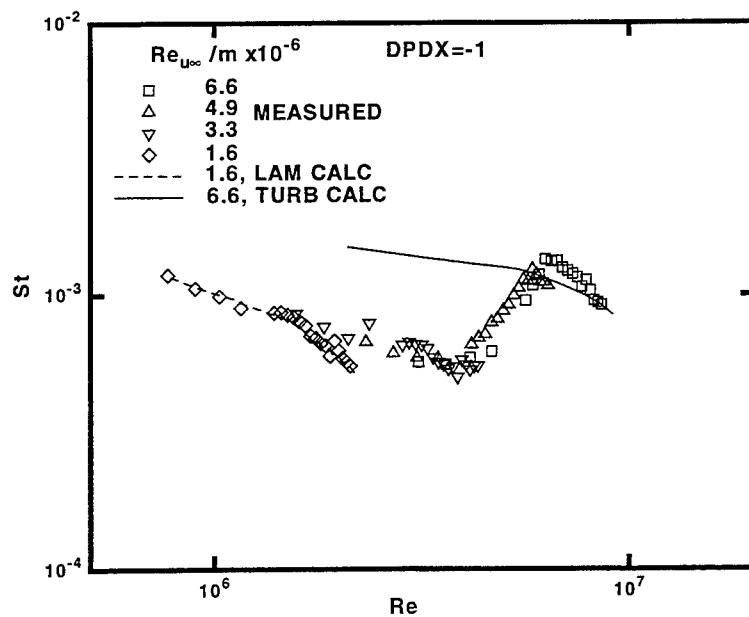Figure 3.12: Heat Transfer, DPDX=0 Configuration.

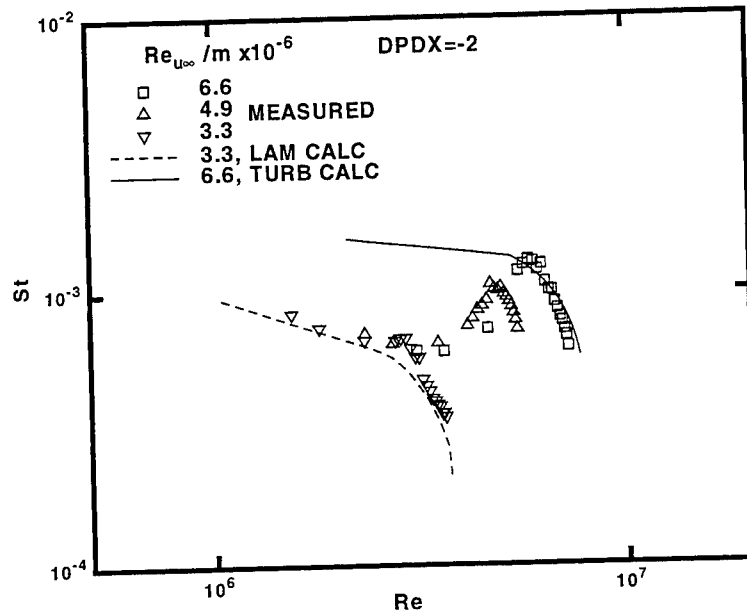Figure 3.13: Heat Transfer, DPDX=-1 Configuration.
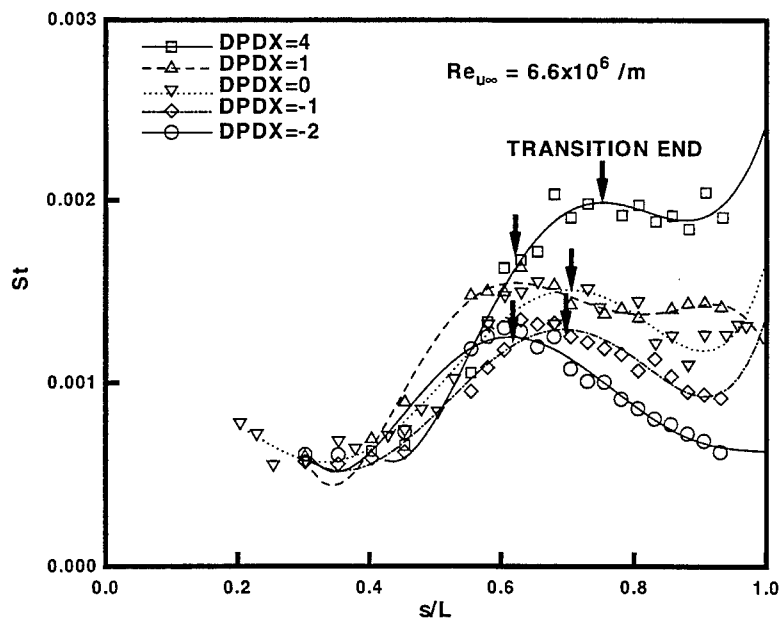
Figure 3.14: Heat Transfer, DPDX=-2 Configuration.

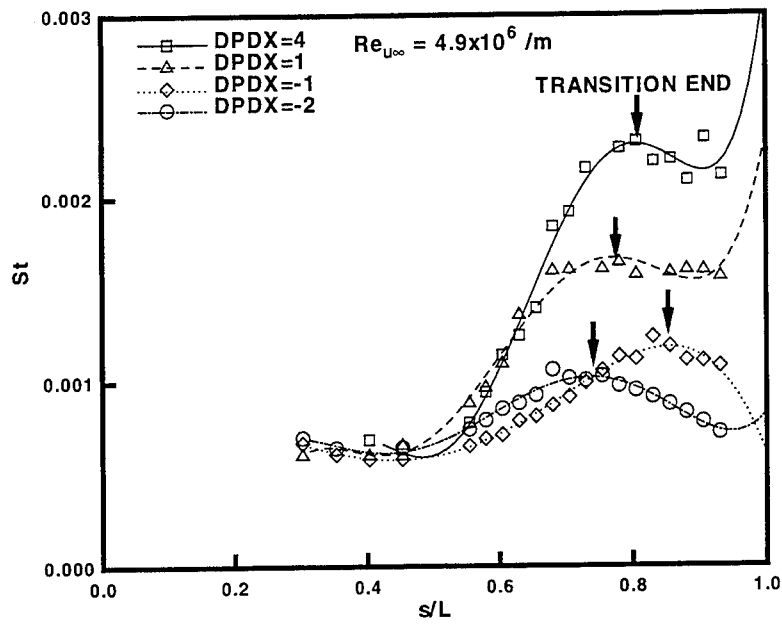Figure 3.15: Heat Transfer, $Re_{u\infty} = 6.6 \times 10^6 \ m^{-1}$.

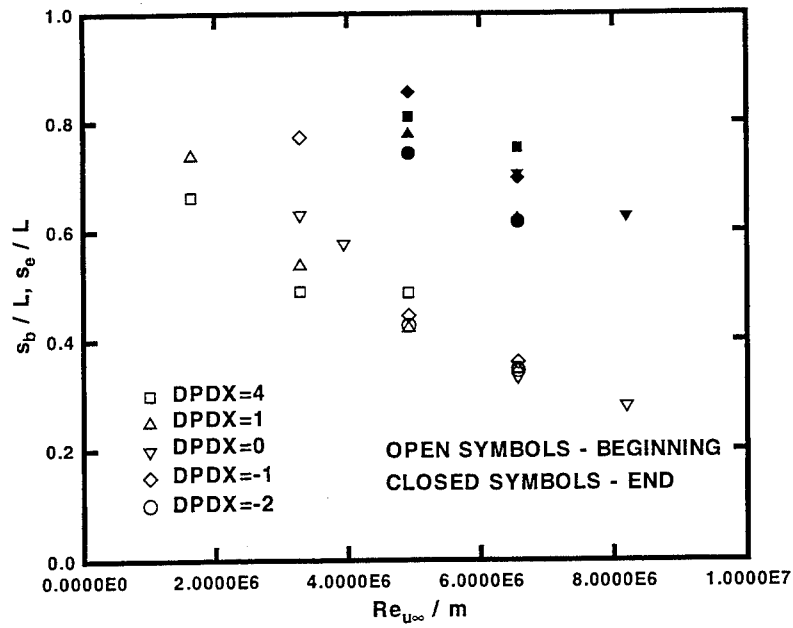Figure 3.16: Heat Transfer, $Re_{u\infty} = 4.9 \times 10^6$ m^{-1}.
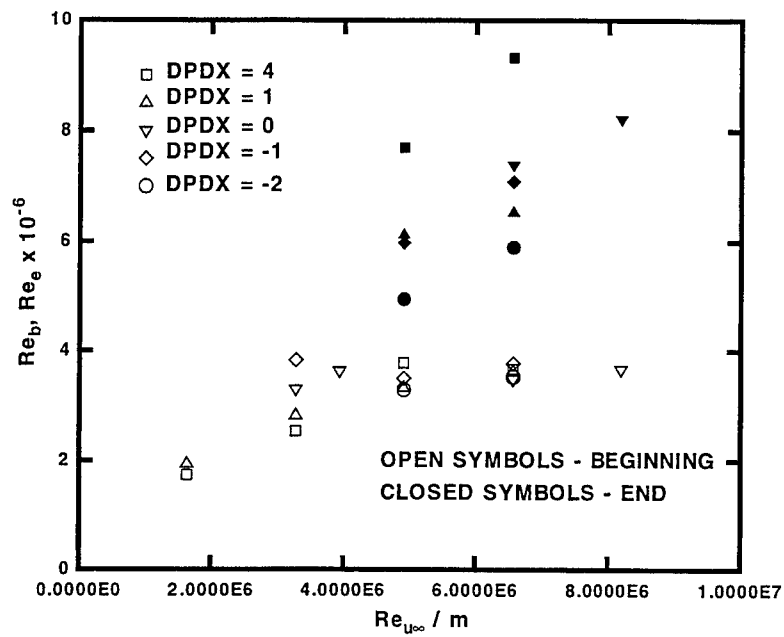

Figure 3.17: Transition Beginning and End.

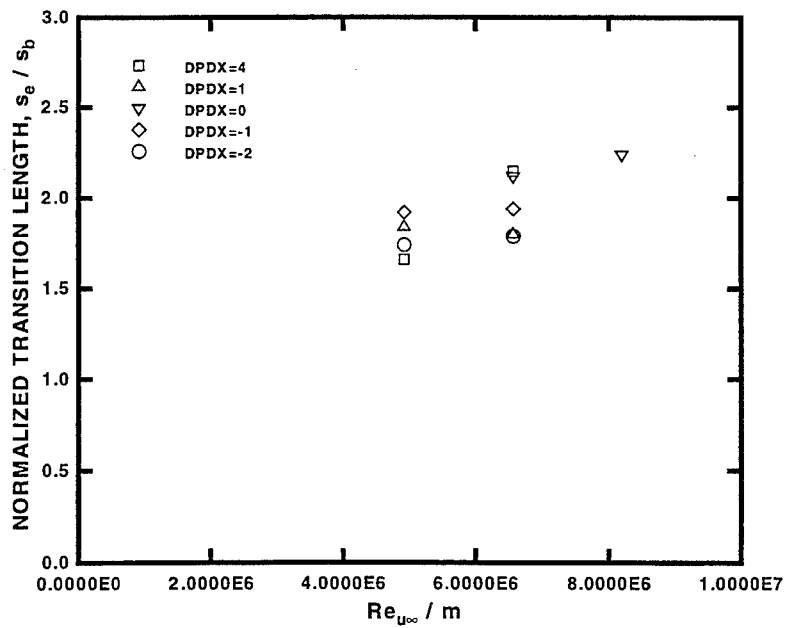Figure 3.18: Transition Reynolds Number Beginning and End.

Figure 3.19: Transition Zone Length.

27
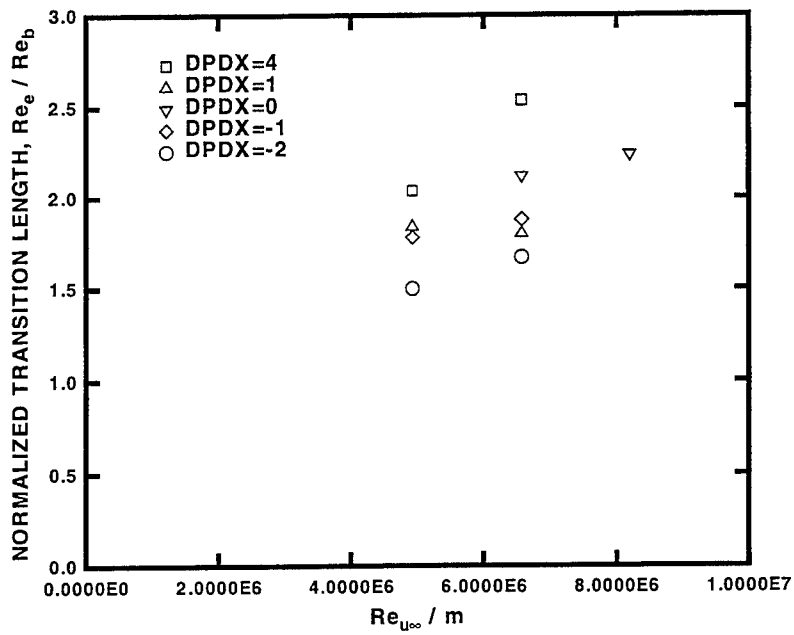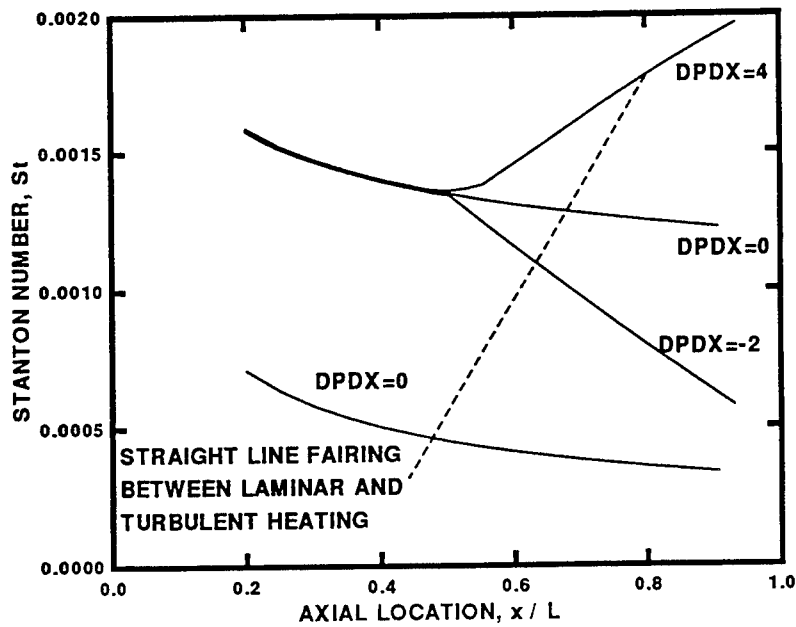
Figure 3.20: Transition Zone Reynolds Number.

Figure 3.21: Effect of End Heat Transfer Level on Transition Zone Length.

28

Section 4

CONCLUSIONS

The end-of-transition on a zero pressure gradient cone at Mach 8 in the AEDC VKF Tunnel B was approximately 2.2 times the laminar length ($s_e/s_b = 2.2$). Although favorable pressure gradient delayed the beginning of transition, the favorable pressure gradient cases tested produced shorter transition lengths than the zero pressure gradient case, about 1.7 to 2.0 times the laminar length. Two adverse pressure gradient cases promoted earlier transition, but transition zone length results for these were inconclusive, although the end-of-transition Reynolds number was somewhat higher than the zero pressure gradient case, primarily due to the increase in edge unit Reynolds number through the compression. In all of the cases cited, transition began in the zero pressure gradient regions of the models, and ended in the pressure gradient regions.

The transition zone length trends are opposite to subsonic trends. One possible cause is that in hypersonic flow, turbulent heat transfer in favorable pressure gradient is lower than zero pressure gradient heat transfer, thus the transitional boundary layer equilibrates to turbulent values more quickly in favorable pressure gradient, and vice versa in adverse pressure gradient. Another possible factor is that the body surface area is growing at a slower rate in the x-direction for the favorable pressure gradient models, thus any turbulent spot would cover the surface more quickly in favorable pressure gradient, and vice versa in adverse pressure gradient.

The present results elucidate to a certain extent the effect of pressure gradients on transition in hypersonic flow, and provide data for comparison to computation. However, the detailed mechanisms of the transition process remain unexplored, and the precise cause of the above-cited results are not certain. Detailed time-resolved and spatial measurements, especially intermittency measurements, are required for a fuller understanding of these

phenomena.

Section 5

REFERENCES

[1] Narasimha, R., "The Laminar-Turbulent Transition Zone in the Boundary Layer," *Prog. in Aerospace Sci.*, vol. 22, pp. 29-80, 1985.

[2] Jack, J. R., "Effect of Favorable Pressure Gradients on Transition for Several Bodies of Revolution at Mach 3.12," NACA TN 4313, July 1958.

[3] Zakkay, V., Bos, A., and Jensen, P. F., Jr., "Laminar, Transitional and Turbulent Flow with Adverse Pressure Gradient on a Cone-Flare at Mach 10," *AIAA J.*, vol. 5, no. 2, February 1967, pp. 201-207.

[4] Emmons, H. W., "The Laminar-Turbulent Transition in a Boundary Layer – Part I," *J. Aero. Sci.* vol. 18, July 1951, pp. 490-498.

[5] Gostelow, J., P., Blunden, A. R., "Investigations of Boundary Layer Transition in an Adverse Pressure Gradient," *ASME Journal of Turbomachinery*, Vol. 111, October 1989, pp. 366-375.

[6] Walker, G. J., Gostelow, J. P., "Effects of Adverse Pressure Gradients on the Nature and Length of Boundary Layer Transition," *ASME Journal of Turbomachinery*, vol. 112, April 1990, pp. 196-205.

[7] Narasimha, R., Devasia, K. J., Gururani, G., and Badri Narayanan, M. A., "On the Distribution of Intermittency in the Transition Region of a Boundary Layer," *Experiments in Fluids*, vol. 2, pp. 171-176, 1984.

[8] Dhawan, S., and Narasimha, R., "Some properties of boundary layer flow during the transition from laminar to turbulent motion,"*J. Fluid Mech.*, vol.3, no.4, 1958, pp. 418-436.

31

[9] Potter, J. L., and Whitfield, J. D., "Effects of slight nose bluntness and roughness on boundary-layer transition in supersonic flows," *J. Fluid Mech.*, vol. 12, no.4, April 1962, pp. 501-535.

[10] Dougherty, N. S., and Fisher, D. F., "Boundary Layer Transition on a 10-Degree Cone: Wind Tunnel / Flight Data Correlation," AIAA-80-0154, January 1980.

[11] Harvey, W. D., and Bobbit, P. J., "Some Anomalies Between Wind Tunnel and Flight Transition Results," AIAA-81-1225, June 1981.

[12] Chen, F. J., "Boundary Layer Transition Extent Measurements on a Cone and Flat Plate at Mach 3.5," AIAA-93-0342, January 1993.

[13] James, C. S., "Observation of Turbulent-Burst Geometry and Growth in Supersonic Flow," NACA TN 4235, April 1958.

[14] Fischer, M. C., "Turbulent Bursts and Rings on a Cone in Helium at M_e=7.6," *AIAA J.*, vol. 10, no. 10, October 1972, pp. 1387-1389.

[15] Havener, A. G., "Detection of Boundary-Layer Transition Using Holography," *AIAA J.*, vol. 15, no. 4, April 1977, pp. 592-593.

[16] Owen, F. K., Horstman, C. C., Stainback, P. C., and R. D. Wagner, "Comparison of Transition and Freestream Disturbance Measurements Obtained in Two Wind Tunnel Facilities," AIAA-74-131, January 1974.

[17] Mack, L. M., "Boundary Layer Stability Theory," *Special Course on Stability and Transition of Laminar Flow*, edited by R. Michel, AGARD Report No. 709, pp. 3-1 to 3-81, 1984.

[18] Papamoschou, D., and Roshko, A., "The compressible turbulent shear layer: an experimental study," *J. Fluid. Mech.*, vol. 197, p. 453.

[19] Richards, B. E., and Stollery, J. L., "Further Experiments on Transition Reversal at Hypersonic Speeds," *AIAA J.*, vol. 4, no. 12, pp. 2224-2226, December 1966.

[20] Cary, A. M., "Turbulent Boundary-Layer Heat Transfer and Transition Measurements for Cold-Wall Conditions at Mach 6," *AIAA J.* vol. 6, no. 5, pp. 958-959, May 1968.

[21] McCauley, W. D., Saydah, A. R., and Bueche, J. F., "Effect of Spherical Roughness on Hypersonic Boundary-Layer Transition," *AIAA J.*, vol. 4, no. 12, pp. 2142-2148, December 1966.

[22] Sanator, "Hypersonic Boundary-Layer Transition Data for a Cold-Wall Slender Cone," *AIAA J.* vol. 3, no. 4, pp.758-760, April 1965.

[23] Dicristina, V., "Three-Dimensional Laminar Boundary Layer Transition on a Sharp 8° Cone at Mach 10," *AIAA J.*, vol. 8, no. 5, May 1970.

[24] Whitfield, J. D., and Iannuzzi, F. A., "Experiments on Roughness Effects on Boundary Layer Transition up to Mach 16," AIAA-68-377, April 1968.

[25] Holloway, P. F., and Sterret, J. R., "Effects of Controlled Surface Roughness on Boundary Layer Transition and Heat Transfer at Mach Numbers of 4.8 and 6.0", NASA TN-D-2054, April 1964.

[26] Beckwith, I. E., and Bertram, M. H., "A Survey of NASA Langley Studies on High-Speed Transition and the Quiet Tunnel," NASA TM-X-2566, July 1972.

[27] Stetson, K. F., "Mach 6 Experiments of Transition on a Cone at Angle of Attack," *J. Spacecraft and Rockets*, vol. 19, no. 5, pp. 397-403, September-October 1982.

[28] Wright, R. L., and Zoby, E. V., "Flight Transition Measurements on a Slender Cone at Mach 20," AIAA-77-719, June 1977.

[29] Berkowitz, A. M., Kyriss, C. L., and Martellucci, A., "Boundary Layer Transition Flight Test Observations," AIAA-77-125, January 1977.

[30] Stetson, K. F., Thompson, E. R., Donaldson, J. C., and Siler, L. G., "Laminar Boundary Layer Stability Experiments on a Cone at Mach 8, Part 1: Sharp Cone," AIAA-83-1761, 1983.

[31] Shope, F. L., "Aerodynamic Design of a Hypersonic Body with a Constant Adverse Pressure Gradient," AIAA-91-3319, September 1991.

[32] Spinetti, R. L., and Shope, F. L., "Aerodynamic Design of a Hypersonic Body with a Constant Favorable Pressure Gradient," AEDC-TMR-91-P15, October 1991.

[33] Truitt, R. W., *Hypersonic Aerodynamics*, p. 64, The Ronald Press Company, New York, 1959.

[34] Stetson, K. F., and Kimmel, R. L., "On Hypersonic Boundary-Layer Stability," AIAA-92-0737, January 1992.

[35] Donaldson, J. C., and Hatcher, M. G., "Investigation of the Development of Laminar Boundary-Layer Instabilities Along a Cooled-Wall Cone in Hypersonic Flows," AEDC-TSR-88-V32, September, 1988.

[36] Demetriades, A., "Hydrodynamic Stability and Transition to Turbulence in a Hypersonic Boundary Layer Over a Sharp Cone," AFOSR TR-75-1435, July 1975.

[37] Smits, A. J., and Smith, D. R., "The Effects of Successive Distortions on the Boundary Layer in a Supersonic Flow," AIAA-92-0309, January 1992.

[38] Stetson, K. F., Thompson, E. R., Donaldson, J. C., and Siler L. G., "Laminar Boundary Layer Stability Experiments on a Cone at Mach 8, Part 3: Sharp Cone at Angle of Attack," AIAA-85-0492, January 1985.

[39] Murray, A. L., "Facilitation of the BLIMP Computer Code and User's Guide," AFWAL-TR-86-3101, January 1987.

[40] Kendall, R. M., Bartlett, E. P., "Nonsimilar Solution of the Multicomponent Laminar Boundary Layer by an Integral-Matrix Method," *AIAA J.*, vol. 6, no. 6, pp. 1089-1097, June 1968.

[41] Stetson, K. F., Thompson, E. R., Donaldson, J. C., and Siler, L. G., "Laminar Boundary Layer Stability Experiments on a Cone at Mach 8, Part 5: Tests with a Cooled Model," AIAA-89-1895, June 1989.

[42] Liepmann, H. W., "Investigation of Boundary Layer Transition on Concave Walls," NACA Wartime Report W87, 1945.

[43] Malik, M., Zang, T., and Bushnell, D., "Boundary Layer Transition in Hypersonic Flows," AIAA-90-5232, October 1990.

[44] Kobayashi, R., and Kohama, K., "Taylor-Görtler Instability of Compressible Boundary Layers," *AIAA J.* vol. 15, no. 12, December 1977.

[45] Floryan, J. M., and Saric, W. S., "Stability of Görtler Vortices in Boundary Layers," *AIAA J.*, vol. 20, no. 3, pp. 316-324, March 1982.

[46] Hall, P., "The Linear Development of Görtler Vortices in Growing Boundary Layers," *J. Fluid Mech.*, vol. 130, pp. 41-58, 1983.

[47] Braslow, A. L., Knox, E. C., and Horton, E. A., "Effect of Distributed Three-Dimensional Roughness and Surface Cooling on Boundary-Layer Transition and Lateral Spread of Turbulence at Supersonic Speeds," NASA TN D-53, 1959.

[48] Gregory, M., "Transition and Spread of Turbulence on a 60 deg Swept-Back Wing," *J. R. Aero. Soc.*, vol. 64, pp. 562-564, 1960.